

Differentially Fed Dual-Polarized SIW Cavity-Backed Patch Antenna with Wide Bandwidth under Multimode Resonance

Jiao-Jiao Xie^{1, 2, *} and Zi Chen²

Abstract—A differentially fed dual-polarized patch antenna with wide bandwidth is presented in this paper using Substrate Integrated Waveguide (SIW) technology. The antenna comprises a circular patch radiator, a square SIW cavity, and four symmetric arc-shaped slots. The circular patch is internally embedded in the square SIW cavity with a surrounded ring slot. Two pairs of differential L-shaped probes are used for the excitation of the differential signals. These signals excite the orthogonal linearly-polarized modes. The dominant resonant mode of the circular patch resonator (TM_{11}) and the modes of the SIW cavity (TE_{110} and TE_{120}/TE_{210}) are employed to achieve effective radiation under these resonances. Besides, four symmetric arc-shaped slots are etched on the top surface of the cavity to enhance the impedance bandwidth. The resonant properties of these modes are studied based on the cavity model theory. Then, their resonant frequencies are discussed to provide information for designing and optimizing such an antenna. Finally, the feeding positions of the differential L-shaped probes are investigated for good impedance matching. The proposed antenna has been fabricated and measured. The measured results show that the proposed antenna achieves a wide impedance bandwidth of about 64.8% (4.37–8.56 GHz) and 64.2% (4.48–8.72 GHz) for horizontal and vertical polarization, respectively. High differential isolation of better than 30 dB and low cross-polarization are obtained by adopting the differential feeding mechanism. Due to the SIW cavity-backed structure, the antenna shows unidirectional radiation patterns and low back-lobe radiation, making it conveniently integrated with microwave differential circuits and applied in the base station systems.

1. INTRODUCTION

With the rapid development of wireless communication, differential circuits are widely used for their advantages of low-noise, high-linearity, and large-dynamic range [1]. Traditional antennas are excited by single feeding port, which makes it bulky when integrated with differential circuits. To overcome the need for baluns, various differential antennas have been investigated. In [2], a differential-fed half-elliptic monopole antenna with triple notched-bands was reported. By introducing rectangular SRRs and an Ω -shaped slot, two operating bands can be notched. A circularly polarized antenna using differential feeding technique was presented in [3]. To generate two operating bands, a parasitic square ring was placed on the rear of the rectangular patch. However, all the afore-mentioned differential antennas possess only one polarization.

Recently, dual-polarized antennas have been widely studied and adopted in wireless base station systems. They can mitigate the multipath fading problem and increase channel capacity by means of polarization diversity [4–6]. For the dual-polarized antennas to work effectively, wide impedance bandwidth, high isolation and low cross-polarization level are required. Nevertheless, they are not easy to accomplish because the input ports are usually highly coupled to each other. This coupling

Received 9 August 2020, Accepted 11 September 2020, Scheduled 27 September 2020

* Corresponding author: Jiao-Jiao Xie (xiejiaojiao@hqu.edu.cn).

¹ College of Information Science and Engineering, Huaqiao University, Xiamen, Fujian 361021, China. ² National Laboratory of Antennas and Microwave Technology, Xidian University, Xi'an, Shaanxi 710071, China.

affects the performance of the antenna and may reduce the impedance bandwidth for each polarization. Substantial efforts have been made to achieve dual-polarized antennas with wide impedance bandwidth and high isolation [7, 8]. A uniplanar UWB polarization antenna with dual notch bands was presented in [9]. With the use of differential feeding structure, high port isolation was achieved. In [10], a dual-polarized UWB-MIMO slot antenna with differential feed scheme was reported. By introducing two pairs of differential ports connected with elliptical patches, high differential port-to-port isolation was obtained. However, most of the proposed antennas were bi-directional radiation types. For this, it is still a challenging task to design a wide dual-polarized patch antenna with stable unidirectional radiation characteristics.

In recent times, substrate integrated waveguide (SIW) cavity has been introduced in antenna design for its advantages of low insertion loss and high radiation efficiency [11, 12]. By using metallic via-holes connecting the top and bottom metal plates, SIW cavity realizes waveguide-based component in planar substrate while maintaining comparable performance. In [13], a quarter-mode substrate integrated waveguide topology was implemented for coaxial-fed antenna to achieve miniaturization. To further reduce the size of the antenna, a L-shaped slot was etched on the top plane of the cavity. Also, a square SIW cavity was proposed to improve the gain of the dual-polarized antenna [14]. The diagonal TE_{120} and TE_{210} modes of the cavity were excited for dual polarization performance. In addition, two rectangular SIW cavities were introduced in [15], the patch mode (TM_{10}) and the cavity modes (TE_{110}/TE_{120}) were excited to resonate at distinct frequencies. Due to the deployment of SIW structure, the antenna-triplexer had a high isolation and unidirectional radiation pattern.

In this paper, a circular patch is internally embedded in the square SIW cavity to construct a wideband dual-polarized patch antenna. Two pairs of differential L-shaped probes are used for the excitation of the orthogonal linearly-polarized signals. As the signal is delivered to the SIW cavity and then coupled to the patch radiator, the cavity modes (TE_{110} and TE_{120}/TE_{210}) incorporating with the patch mode (TM_{11}) are excited simultaneously. By etching four symmetric arc-shaped slots on the top surface of the cavity, wide impedance bandwidth can be obtained. Due to the introduction of the SIW cavity, good electrical characteristics such as unidirectional radiation pattern and stable gain can be achieved. Details of the antenna design and experimental results are presented and analyzed.

2. ANTENNA CONFIGURATION

The configuration of the proposed differentially fed dual-polarized SIW cavity-backed patch antenna and its detailed dimensions are shown in Figure 1. The antenna is composed of a circular patch, a square SIW cavity with a circular aperture, four symmetric arc-shaped slots and two pairs of differential L-shaped probes. The circular patch with a distance of $0.103\lambda_0$ (λ_0 is the free space wavelength at the center frequency) from the ground plane is printed on a 1-mm-thick Rogers 5870 substrate. The square SIW cavity is formed by connecting the top and bottom copper claddings with metallic pins, which form the lateral conducting walls. A circular aperture is etched in the middle of the SIW cavity for embedding the circular patch. To enhance the impedance bandwidth, four arc-shaped slots are placed on the top surface of the cavity. These two slot pairs are orthogonal to each other along the aperture edge. With the help of two pairs of differential L-shaped probes, the orthogonal dual linearly-polarized modes can be obtained. Each pair of L-shaped probes are excited with the equal amplitudes and 180° phase difference, which can reduce the cross-polarization level. When differential port 1 is excited and differential port 2 is connected to a match load, the antenna is 0° polarization (similarly differential port 2 excites 90° polarized wave). The key parameters are optimized using Ansoft High Frequency Structure Simulator (HFSS) software.

To illustrate the design methodology, the resonant properties of the circular patch resonator are investigated firstly. According to the cavity model theory, the fundamental TM_{11} mode is selected as the working mode of the circular patch. The radius of the circular patch can be calculated using the equation suggested as [16]

$$f_{mn} = \frac{cK_{mn}}{2\pi r_1 \sqrt{\varepsilon_{eff}}} \quad (1)$$

where c is the velocity of light in the free space, and ε_{eff} is the effective dielectric constant of the substrate. K_{mn} represents the corresponding root of Bessel's function and its value for the TM_{11} mode

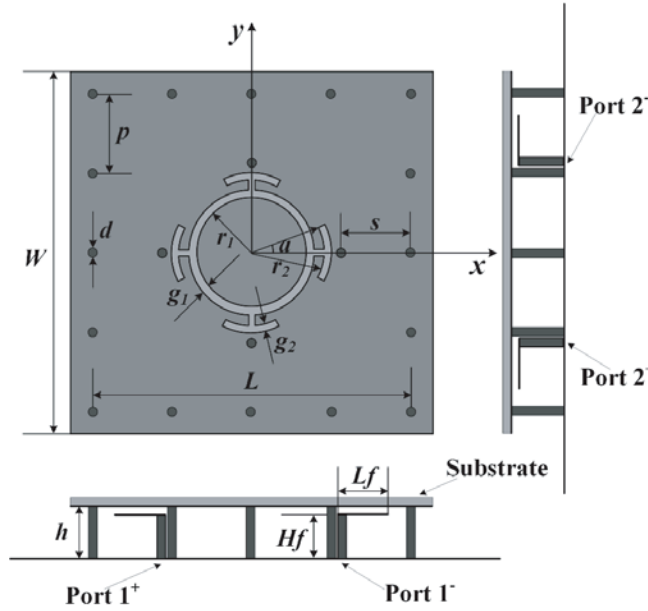


Figure 1. Antenna configuration and detailed dimensions.

is 1.84.

Then, the resonant properties of the square SIW cavity are studied. As the SIW is essentially a quasi-waveguide structure and its cavity is surrounded by post walls, the expression given for rectangular waveguide cavity is suitable for the discussed square SIW cavity. Thus, the dimension of the square SIW cavity can be deduced from the waveguide equivalence model [17]

$$f_{mn0} = \frac{c}{2\sqrt{\mu\epsilon}} \sqrt{\left(\frac{m}{L}\right)^2 + \left(\frac{n}{L}\right)^2} \quad (2)$$

where m and n are two nonnegative integers, while L is the side length of the square SIW cavity. It has been estimated to support TE_{110} and TE_{120}/TE_{210} modes, respectively.

3. ANTENNA DESIGN

3.1. Antenna Mechanism

To explain the operating mechanism, three antennas, namely, Antennas I–III, are used herein as reference antennas for demonstration of the proposed antenna as shown in Figure 2. The design starts with Antenna I and II, which are circular patch resonator and square SIW cavity with a surrounded aperture. The same dimensions are used for all these antennas.

In the case of Antenna I, a circular patch is chosen as the radiation patch. The radius of the patch is adjusted such that the patch radiates in the fundamental TM_{11} mode and resonates at 7 GHz. The corresponding field distribution is shown in Figure 3. It is found TM_{11} is odd mode and the maximum field concentrates in the outer edge of the circular patch. In the case of Antenna II, a circular aperture is etched in the middle of the square SIW cavity. Due to aperture loading, the cavity modes (TE_{110} and TE_{120}/TE_{210}) get perturbed and generate the modified modes TE_{110} and TE_{120}/TE_{210} toward the higher frequencies at 5.2 and 7.6 GHz, respectively. Their field distributions are shown in Figure 4. It can be found that the original cavity mode TE_{110} is influenced significantly by the aperture and maximum field is concentrated in the outer shortened aperture of the cavity. On the other hand, field distribution of the original TE_{120}/TE_{210} mode is slightly influenced by the slot. The modified TE_{120}/TE_{210} is odd mode and the maximum field concentrates in the shortened outer aperture.

Thus, Antenna III can be constructed by embedding the circular patch in the square aperture of the SIW cavity. Its differential reflection coefficient is depicted in Figure 5. The expected modes in

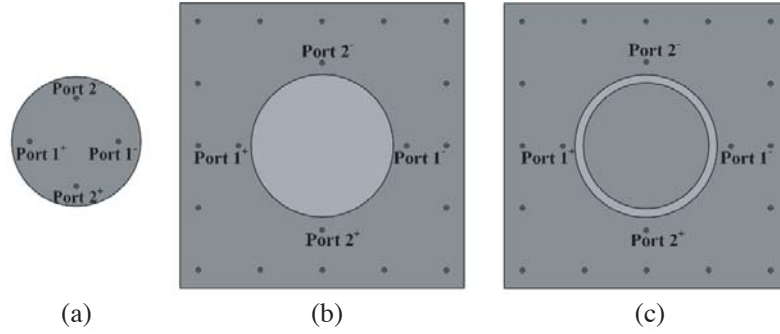


Figure 2. Configurations of three reference antennas. (a) Antenna I. (b) Antenna II. (c) Antenna III.

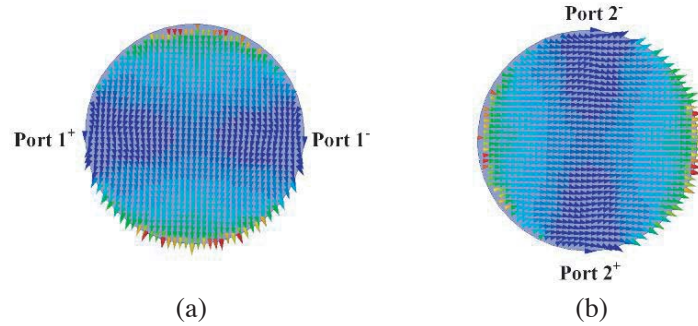


Figure 3. Simulated H -field distributions in Antenna I at 7 GHz. (a) TM_{11} mode (differential port 1 excitation). (b) TM_{11} mode (differential port 2 excitation).

Antenna I and II are all generated in Antenna III. Meanwhile, three resonant frequencies are obtained over the simulated frequency band. Due to the nested configuration, an additional shunt capacitance is generated which affects the resonant properties of the antenna. To compensate this and achieve good impedance matching, the proposed antenna shown in Figure 1 is constructed. Four symmetric arc-shaped slots are etched on the top surface of the cavity. The introduction of arc-shaped slots changes the field distribution inside the cavity, which lowers the resonant frequencies of the modes TE_{110} and TM_{11} . As a result, the impedance bandwidth of the proposed antenna can be improved.

The simulated field distributions of the proposed antenna at three resonant frequencies of 4.9, 6.1, and 7.9 GHz are shown in Figure 6. At the lower and higher frequencies (4.9 and 7.9 GHz), the field is concentrated around the SIW cavity, thus successfully exciting the modified cavity modes TE_{110} and TE_{120}/TE_{210} . At the middle frequency (6.1 GHz), the field is focused on the edge of the circular patch, thereby indicating effective excitation of the modified patch mode TM_{11} . Meanwhile, when one of the differential ports is excited, there is hardly field distribution at the other differential port. This leads to high isolation between the differential ports.

3.2. Parameter Analysis

To analyze the effects of the key structure parameters on the antenna performance, a parametric study is performed with HFSS. When one parameter is studied, the others are kept constant. Because of the symmetrical configuration, only S_{dd11} is presented in this section.

At first, the function of the circular patch is studied. Figure 7 shows the simulated differential reflection coefficient of the proposed antenna for various r_1 . As r_1 increases from 7.5 mm to 9.5 mm, it is observed that the lower and middle resonant frequencies shift down dramatically, while the higher resonant frequency changes slightly. This shift is found due to increment in the dimension of the circular patch and extension in the effective aperture of the SIW cavity. In addition, a larger r_1 worsens the impedance matching in the whole operating band. Thus, $r_1 = 7.5$ mm was chosen as the length of the circular patch for good impedance matching.

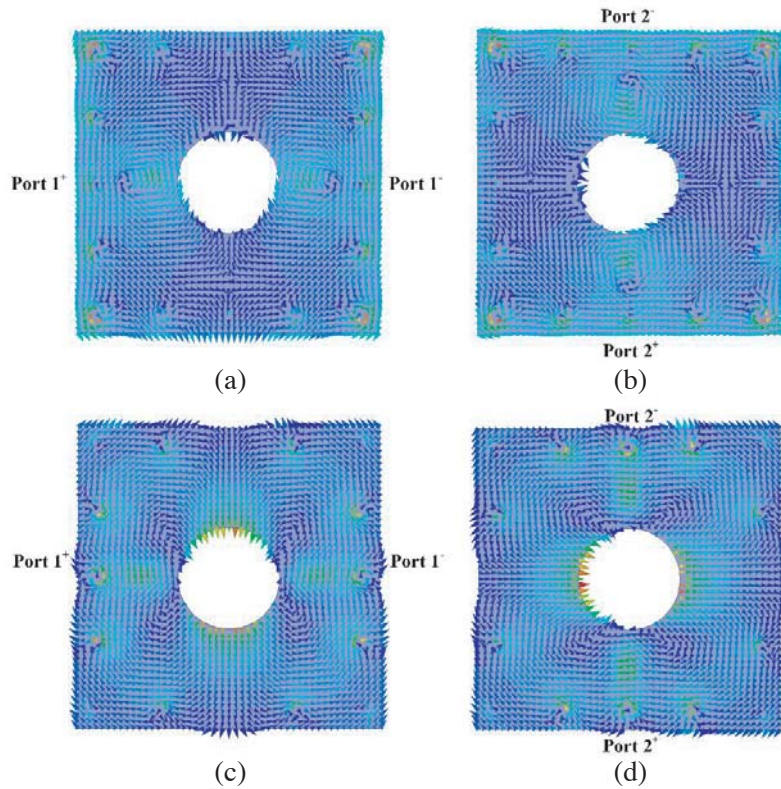


Figure 4. Simulated H -field distributions in Antenna II. (a) Modified TE_{110} mode at 5.2 GHz (differential port 1 excitation). (b) Modified TE_{110} mode at 5.2 GHz (differential port 2 excitation). (c) Modified TE_{120} mode at 7.6 GHz (differential port 1 excitation). (d) Modified TE_{210} mode at 7.6 GHz (differential port 2 excitation).

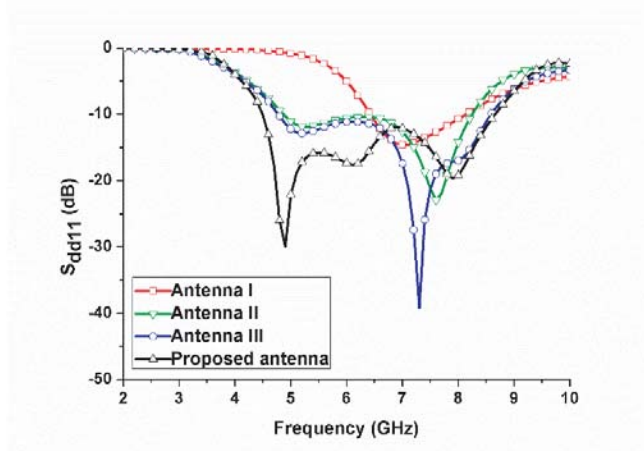


Figure 5. Simulated differential reflection coefficients of referenced Antenna I, II, III and the proposed antenna.

Then, the function of the arc-shaped slot is demonstrated. The simulated differential reflection coefficient of the proposed antenna for various a is given in Figure 8. It observes a minor change in the higher band while the lower and middle bands are strongly affected. In fact, changing a will lead to the variations of current path, which directly affect the coupling between the circular patch and SIW cavity. Additionally, over increasing the length of the arc-shaped slot will cause poorer impedance matching in the whole operating band. Thus, $a = 18^\circ$ was chosen for good impedance matching.

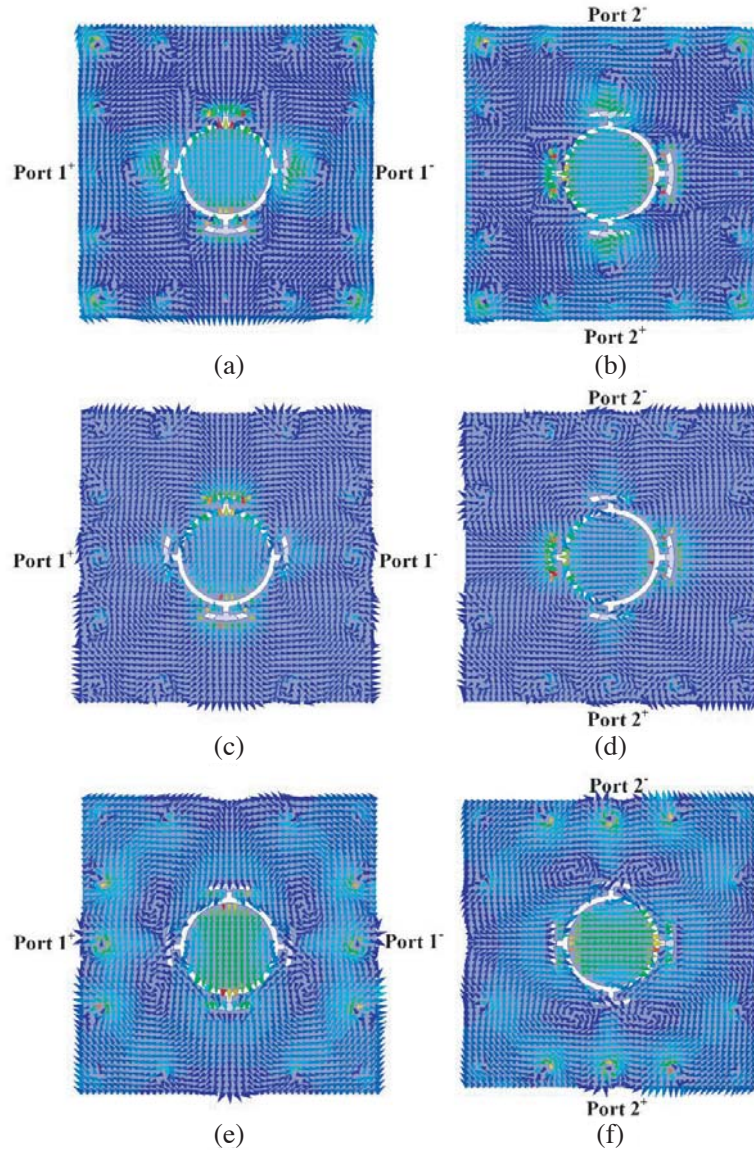


Figure 6. Simulated H -field distributions in the proposed antenna. (a) Modified TE_{110} mode at 4.9 GHz (differential port 1 excitation). (b) Modified TE_{110} mode at 4.9 GHz (differential port 2 excitation). (c) Modified TM_{11} mode at 6.1 GHz (differential port 1 excitation). (d) Modified TM_{11} mode at 6.1 GHz (differential port 2 excitation). (e) Modified TE_{120} mode at 7.9 GHz (differential port 1 excitation). (f) Modified TE_{210} mode at 7.9 GHz (differential port 2 excitation).

Moreover, the effect of the SIW cavity on the antenna performance is illustrated. Figure 9(a) shows the simulated differential reflection coefficient of the proposed antenna for various L . From the graph, it is clearly visible that the lower and higher resonant frequencies are very sensitive to the length of the SIW cavity. When L increases from 43 mm to 45 mm, both the lower and higher resonant frequencies decrease, due to increment in the dimension of the SIW cavity. Therefore, L was selected to be 44 mm for good impedance matching and compact structure. In addition, the simulated differential reflection coefficient of the proposed antenna for various h is given in Figure 9(b). As h increases from 4.7 mm to 5.5 mm, the middle resonant frequency shift down dramatically, while the lower and higher resonant frequencies change slightly. Meanwhile, a thicker height gives wider impedance bandwidth. However, over increasing the height of the SIW cavity will cause poorer impedance matching in the higher band. Thus, h was selected to be 5.1 mm for good impedance matching.

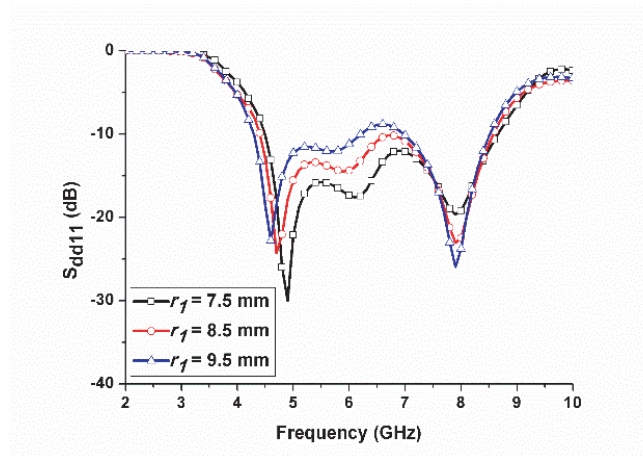


Figure 7. Effect of the circular patch (r_1) on the resonant frequencies.

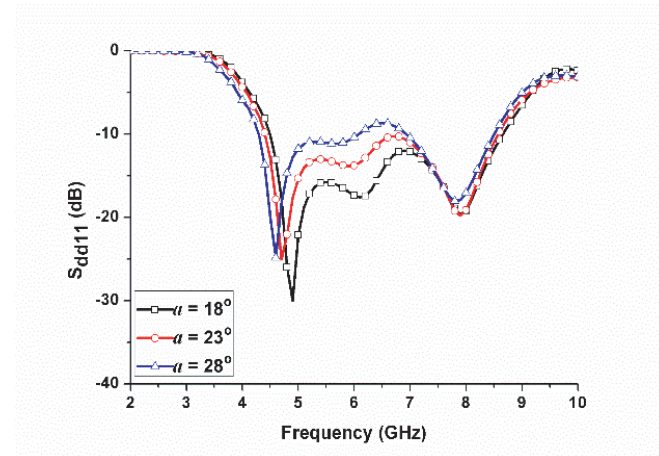
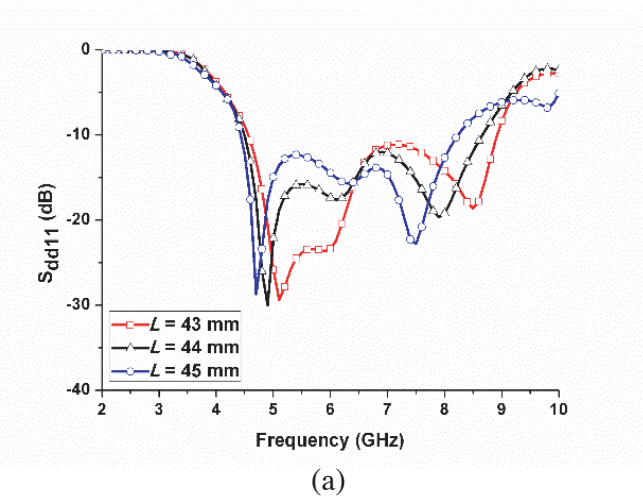
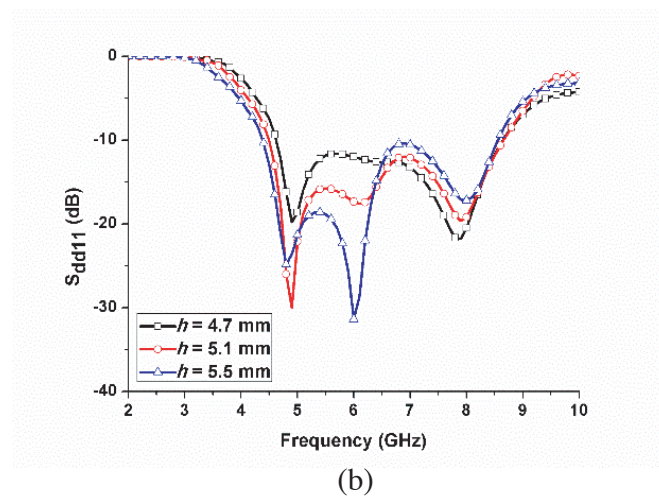


Figure 8. Effect of the arc-shaped slot (a) on the resonant frequencies.



(a)



(b)

Figure 9. Effect of the SIW cavity on the antenna performance. (a) Length of the SIW cavity (L). (b) Height of the SIW cavity (h).

Furthermore, to illustrate the effect of the pitch of metallic pins, the simulated radiation gain at resonant frequencies of the discussed modes for various p is given in Figure 10(a). As shown in the graph, when p is enlarged from 5.5 mm to 22 mm, the radiation gain of TM_{11} decreases at first and then rises slowly, while the gain of TE_{110} and TE_{120} decrease at first and then hover around 6.9 and 7.8 dBi, respectively. Additionally, Figure 10(b) shows the simulated differential reflection coefficient of the proposed antenna for various p . As p increases from 5.5 mm to 22 mm, both the lower and higher resonant frequencies decrease, while the middle resonant frequency changes slightly. A larger p gives wider impedance bandwidth. However, over increasing the pitch of metallic pins will cause poorer impedance matching in the lower band. Thus, p was selected to be 11 mm for stable radiation gain and wide impedance bandwidth. Moreover, the effect of the diameter of metallic pins (d) on the antenna performance is demonstrated in Figure 11. From the graph, it is observed that the diameter of metallic pins has a significant effect on the impedance bandwidth. A smaller d gives wider impedance bandwidth. Therefore, d was selected to be 1 mm for wide impedance bandwidth.

Finally, the influence of the differential L-shaped probes on the antenna performance is exhibited. Figure 12 shows the simulated differential reflection coefficient of the proposed antenna for various s .

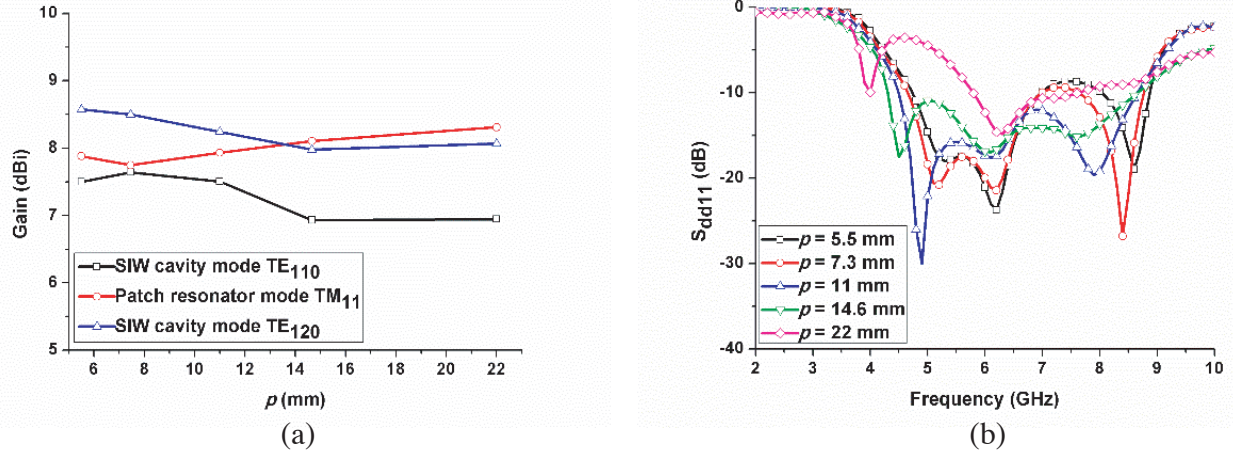


Figure 10. Effect of the pitch of pins (p) on the antenna performance. (a) Radiation gain. (b) S_{dd11} .

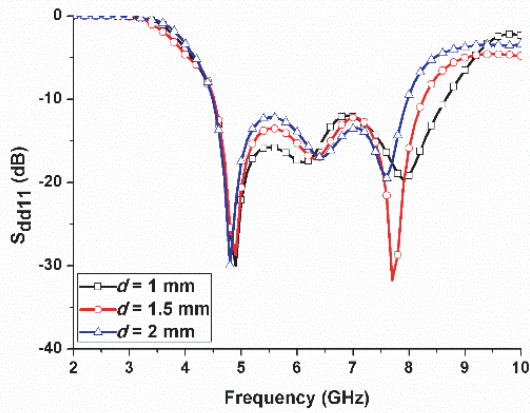


Figure 11. Effect of the diameter of pins (d) on the antenna performance.

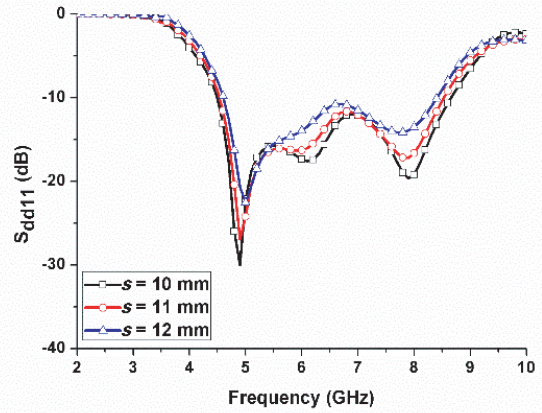


Figure 12. Effect of the differential probes (s) on the antenna performance.

As can be seen, the position of the feeding probes has a significant effect on the antenna performance. A smaller position s gives better impedance matching in the higher band. This is because the input impedance varies with different positions of feeding point. But we also find that the resonant frequencies stay stable against the s , especially in the lower band. The reason is that resonant frequencies are decided by the sizes of the circular patch and SIW cavity. Therefore, s was selected to be 10 mm good impedance matching.

4. RESULTS AND DISCUSSION

To validate the presented design method, a prototype of the proposed antenna shown in Figure 13 is fabricated. The optimum dimensional parameters are: $W = 50$ mm, $L = 44$ mm, $h = 5.1$ mm, $Hf = 3.9$ mm, $Lf = 6$ mm, $s = 10$ mm, $p = 11$ mm, $d = 1$ mm, $g_1 = 1$ mm, $g_2 = 0.8$ mm, $r_1 = 7.5$ mm, $r_2 = 10$ mm, and $a = 18^\circ$. The antenna is measured with WILTRON 37269A vector network analyzer and a fully automated anechoic chamber. Figure 14 shows the simulated and measured differential reflection coefficients of the proposed antenna. Due to the symmetry property of the antenna configuration, the simulated results for differential ports 1 and 2 are identical. The simulated

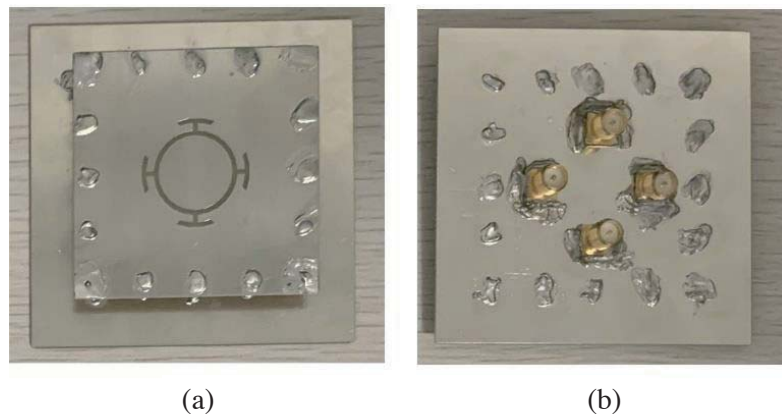


Figure 13. Photograph of the fabricated prototype. (a) Top view. (b) Bottom view.

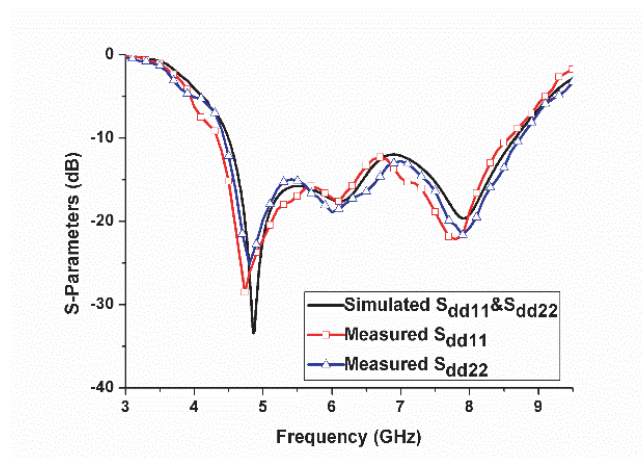


Figure 14. Simulated and measured S_{dd11}/S_{dd22} of the proposed antenna.

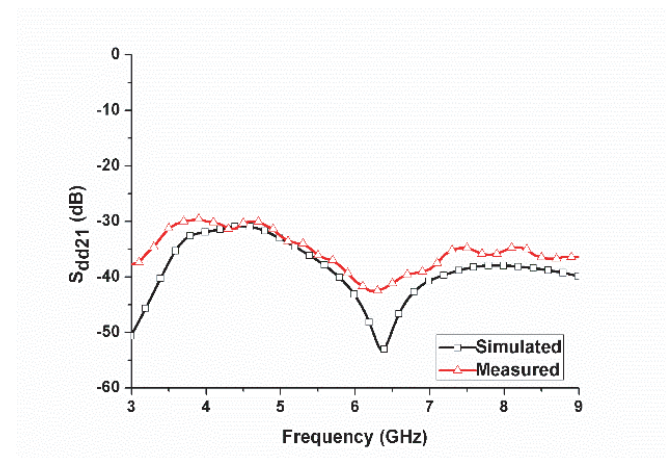


Figure 15. Simulated and measured S_{dd21} of the proposed antenna.

–10 dB impedance bandwidth of the proposed antenna is 62.9% (4.51–8.65 GHz). The measured –10 dB impedance bandwidth of the proposed antenna is 64.8% (4.37–8.56 GHz) and 64.2% (4.48–8.72 GHz) for horizontal and vertical polarization, respectively, both covering the 5.2/5.8 GHz wireless local area network (WLAN) and the 5.5 GHz WiMAX bands. Good agreement between simulation and measurement of impedance bandwidth can be observed. A slight discrepancy between the two measured differential ports can be attributed to the fabrication imperfection. The simulated and measured differential isolation is shown in Figure 15. It can be seen that the isolation is better than 30 dB in the whole operating band.

The measured radiation patterns of the proposed antenna at 4.9, 6.1, and 7.9 GHz are plotted in Figure 16. To measure the radiation pattern of the differential antenna, a 180° hybrid coupler is used for the generation of differential signals. When port 1 is differential excited, port 2 is connected to a match load for 0° polarization (similarly port 2 excites 90° polarization mode). As shown in the figures, there is a dip in the broadside direction at 4.9 GHz, which is caused due to cancellation of the fields of the equal amplitude and differential phase across the arc-shaped slots. On the other hand, the radiation patterns at the resonant frequencies of 6.1 and 7.9 GHz are unidirectional. The main beam of the radiation is always fixed in the broadside direction. It is caused by the introduction of the cavity-backed configuration, which can reinforce the radiating power in the broadside direction and suppress it in the back side. The overall front-to-back-ratio is better than 17.3 dB for each resonant frequency. Additionally, the cross-polarization levels at both differential ports are less than –32 dB

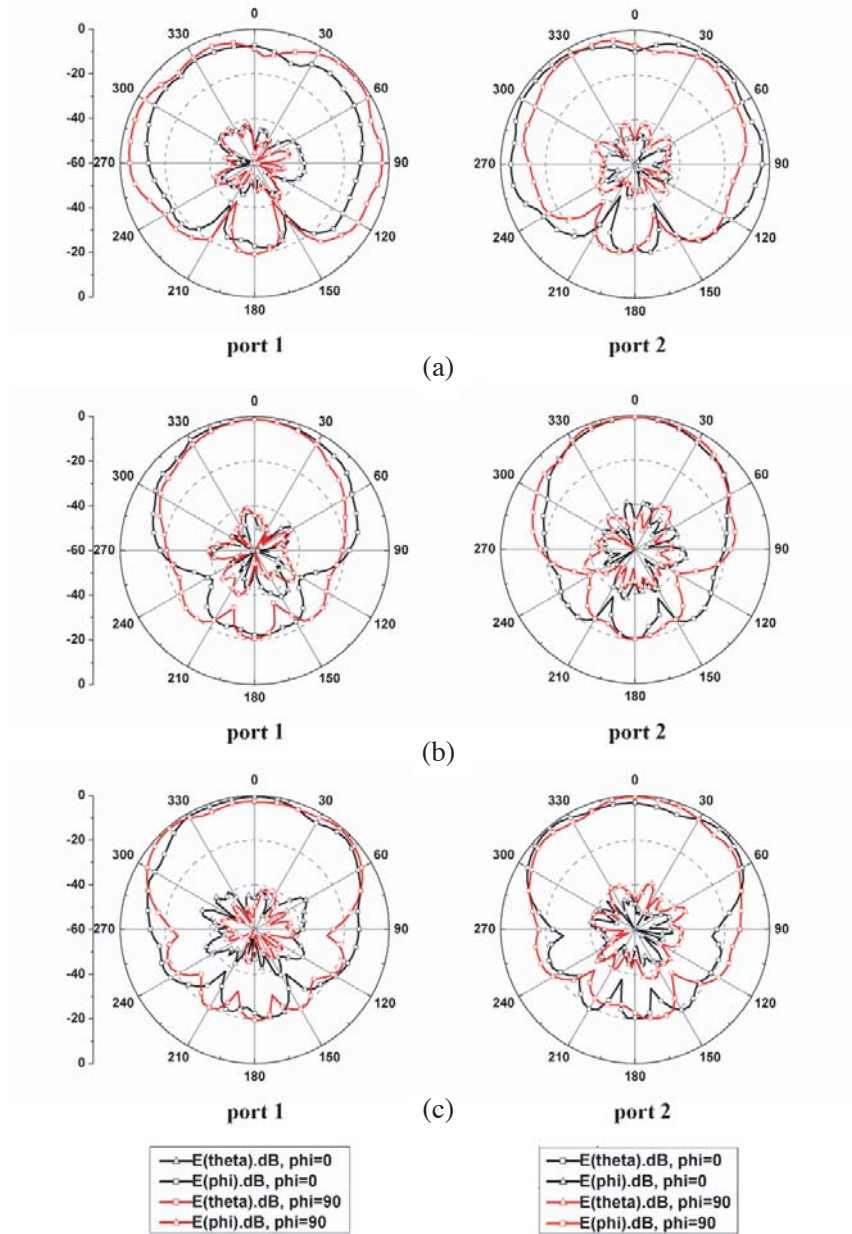


Figure 16. Measured radiation patterns of the proposed antenna at (a) 4.9 GHz, (b) 6.1 GHz, and (c) 7.9 GHz.

within the main lobe.

Figure 17 gives the simulated and measured gains of the proposed antenna in the whole operating band. Good agreement between the simulated and measured results is obtained. A slight difference between them is mainly caused by the unexpected losses in the feeding circuit and SMA probes. When differential port 1 is excited, the measured gain is about 7.4 dBi for 0° polarization. When differential port 2 is excited, the measured gain is about 7.6 dBi for 90° polarization. There is a little difference between two differential ports, which may be caused by the asymmetric factors brought in the fabrication process.

To highlight the contribution of the proposed antenna, a performance comparison with the previous dual-polarized antennas is presented in Table 1. It can be observed that the proposed antenna offers a better impedance bandwidth compared to the other dual-polarized antennas by using multimode resonance.

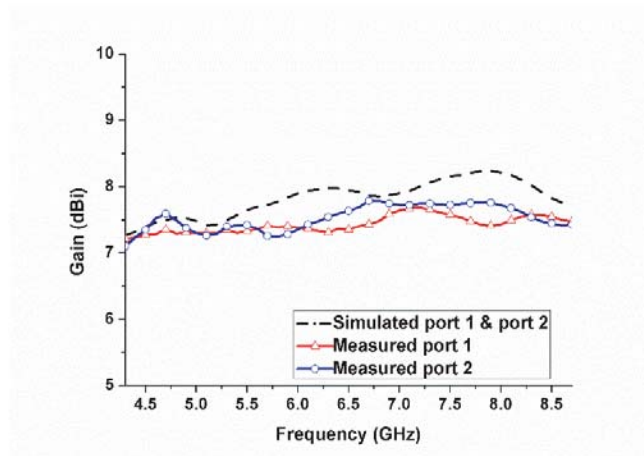


Figure 17. Simulated and measured gains of the proposed antenna.

Table 1. Performance comparison of the proposed antenna with the previous dual-polarized antennas using differential feeding technique.

Antenna	SIW	Bandwidth	Isolation	Cross-pol level	Gain
Ref. [5]	No	2.1%	98 dB	50 dB	4 dBi
Ref. [6]	No	9.9%	43 dB	No discuss	5.6 dBi
Ref. [7]	No	19.3%	43 dB	30 dB	8.1 dBi
Ref. [8]	No	48%	35 dB	20 dB	7.9 dBi
Ref. [14]	Yes	2.3%	70 dB	32 dB	7.4 dBi
Proposed	Yes	64.2%	30 dB	32 dB	7.4 dBi

5. CONCLUSION

This paper has proposed a differentially fed dual-polarized patch antenna based on the patch resonator and SIW cavity. Owing to the multimode resonance, wide bandwidth is achieved. To improve the impedance matching, four symmetric arc-shaped slots are etched on the top surface of the cavity. The proposed antenna is excited by two pairs of L-shaped probes with the equal amplitudes and 180° phase difference. When it is connected to microwave differential circuits, the balun is not needed. The resonant properties of the patch mode (TM_{11}) and cavity modes (TE_{110} and TE_{120}/TE_{210}) are studied to provide information for designing and optimizing such an antenna. Due to its wide impedance bandwidth, high isolation, and unidirectional radiation pattern, the proposed antenna is suitable for base station systems with the differential circuits.

REFERENCES

1. Kang, B., H. Hwang, and C. Park, "Differential transformer using bonder-wires and patterns on a printed circuit board for RF circuit applications," *Progress In Electromagnetics Research*, Vol. 135, 363–371, 2013.
2. Xu, Y., H. Li, Y.-Z. Yin, and Z. Deng, "A compact differential-fed half-elliptic monopole antenna with triple band-notched function," *Progress In Electromagnetics Research Letters*, Vol. 62, 35–40, 2016.
3. Wu, J., Y.-Z. Yin, Z. Wang, and R. Lian, "Dual-band circularly polarized antenna with differential feeding," *Progress In Electromagnetics Research C*, Vol. 49, 11–17, 2014.

4. Yang, M., J. Zhou, W. Lian, and B. Chen, "Dual-band dual-polarized magneto-electric dipole antenna with dual-layer structure," *Progress In Electromagnetics Research M*, Vol. 92, 193–202, 2020.
5. Nawaz, H. and I. Tekin, "Duble-differential-fed, dual-polarized patch antenna with 90 dB interport RF isolation for a 2.4 GHz in-band full-duplex transceiver," *IEEE Antennas Wireless Propagat. Lett.*, Vol. 17, 287–290, 2018.
6. Tang, H., C. Tong, and J.-X. Chen, "Differential dual-polarized filtering dielectric resonator antenna," *IEEE Trans. Antennas Propag.*, Vol. 66, 4298–4302, 2018.
7. Liu, Y., S. Wang, X. Wang, and Y. Jia, "A differentially fed dual-polarized slot antenna with high isolation and low profile for base station application," *IEEE Antennas Wireless Propagat. Lett.*, Vol. 18, 303–307, 2019.
8. Tang, Z., J. Liu, and Y. Yin, "Enhanced cross-polarization discrimination of wideband differentially fed dual-polarized antenna via a shorting loop," *IEEE Antennas Wireless Propagat. Lett.*, Vol. 17, 1454–1458, 2018.
9. Huang, H., Y. Liu, and S.-X. Gong, "Differential-fed ultrawideband polarization diversity antenna with dual notch bands," *Microw. Opt. Technol. Lett.*, Vol. 57, 1084–1089, 2015.
10. Li, W.-A., Z.-H. Tu, and Q.-X. Chu, "Compact, high isolation, and dual-polarized differential dual-notched UWB-MIMO slot antenna," *Microw. Opt. Technol. Lett.*, Vol. 57, 2609–2614, 2015.
11. Dokuparthi, J. and A. Sudhakar, "Dual band half mode SIW semi circular cavity back slot antenna," *Progress In Electromagnetics Research Letters*, Vol. 87, 7–14, 2019.
12. Pavone, S. C. and M. Albani, "Design and fabrication of a sectoral beam slotted antenna in SIW technology for surveillance applications at millimeter waves," *Progress In Electromagnetics Research*, Vol. 167, 55–65, 2020.
13. Chaturvedi, D. and S. Raghavan, "Compact QMSIW based antennas for WLAN/WBAN applications," *Progress In Electromagnetics Research C*, Vol. 82, 145–153, 2018.
14. Srivastava, G. and A. Mohan, "A differential dual-polarized SIW cavity-backed slot antenna," *IEEE Trans. Antennas Propag.*, Vol. 67, 3450–3454, 2019.
15. Chaturvedi, D., A. Kumar, and S. Raghavan, "An integrated SIW cavity-backed slot antenna-triplexer," *IEEE Antennas Wireless Propagat. Lett.*, Vol. 17, 1557–1560, 2018.
16. Wu Q., H. Wang, C. Yu, and W. Hong, "Low-profile circularly polarized cavity-backed antennas using SIW techniques," *IEEE Trans. Antennas Propag.*, Vol. 64, 2832–2839, 2016.
17. Liu Q., L. Zhu, J. Wang, and W. Wu, "Wideband low-profile differential-fed patch antennas with an embedded SIW cavity under dual-mode resonance," *IEEE Trans. Antennas Propag.*, Vol. 67, 4235–4240, 2019.